Biphasic Lu3MgAl3SiO12-based Transparent Ceramics for highly Uniform Laser-Diode-driven White Lighting

Shaowei Feng, Yongchang Guo, Mathieu Allix, Shuxing Li, Rong-Jun Xie, Jie Fu, Cécile Genevois, Emmanuel Véron, Hui Wang, Yafeng Yang, et al.

Biphasic $Lu_3MgAl_3SiO_{12}$-based Transparent Ceramics for highly Uniform Laser-Diode-driven White Lighting

Shaowei Feng [1,2,3], Yongchang Guo [1,2,3], Mathieu Allix [4,], Shuxing Li [5], Rong-Jun Xie [5], Jie Fu [2,3], Cécile Genevois [4], Emmanuel Véron [4], Hui Wang [2], Yafeng Yang [2,3], Haiming Qin [6,*], Jianqiang Li [1,7 *]*

[1] *School of Materials Science and Engineering, University of Science and Technology Beijing, Beijing 100083, P. R. China*

[2] *Institute of Process Engineering, Chinese Academy of Sciences, Beijing 100190, P. R. China*

[3] *University of Chinese Academy of Sciences, Beijing 100049, P. R. China*

[4] *CNRS, CEMHTI UPR 3079, Univ. Orléans, 45071 Orléans, France.*

[5] *College of Materials, Xiamen University, Simingnan-Road 422, Xiamen 361005, P. R. China*

[6] *Ningbo Institute of Materials Technology and Engineering, Chinese Academy of Sciences, Ningbo 315201, P. R. China*

[7] *Lead contact*

*Correspondence:

jianqiangli@ustb.edu.cn (J. L.),

allix@cnrs-orleans.fr (M. A.),

qinhaiming@nimte.ac.cn (H. Q)

Summary

$Lu_3Al_5O_{12}:Ce^{3+}$ is a promising color converter for laser diode- (LD-) driven solid-state lighting and displays due to the improved thermal stability of its luminescence compared to widely-used $Y_3Al_5O_{12}:Ce^{3+}$ materials. However, LuAG:Ce^{3+} emits green light, which is a severe drawback for white lighting applications. Here, we report new biphasic $Lu_3MgAl_3SiO_{12}:Ce^{3+}$ (BP-LMAS:Ce^{3+}) transparent ceramics that exhibit red-shifted emission via the inclusion of a secondary phase $(Lu/Mg)_4(Al/Si)_2O_9$. This phase, dispersed homogeneously in the BP-LMAS:Ce^{3+} matrix, provides scattering centers which improve the uniformity of the emitted light. The material demonstrates a broad orange-yellow emission band centered at 564 nm (450 nm excitation), internal quantum efficiency of 76.1% and transmittance of 76%, and enhanced thermal stability. Under excitation of 14.5 W mm^{-2} blue LDs, it generates white light with a high luminous flux of 5655 lm. This demonstrates that BP-LMAS:Ce^{3+} transparent ceramics are promising candidates as color conversion materials for LD-driven white lighting applications.

Keywords: $Lu_3Al_5O_{12}$, Transparent Ceramics, Secondary Phase, Mg^{2+}-Si^{4+} Substitution, LDs-driven Lighting, Scattering Centers

INTRODUCTION

The past few decades have witnessed tremendous progress in developing light-emitting diodes (LEDs) now widely used in modern lighting technology and backlight displays.[1,2] As a matter of fact, solid-state white lighting that uses blue-emitting LEDs as an excitation light source has rapidly evolved in popularity to promote power-saving and lower pollution.[3,4] However, LEDs have an innate non-thermal "efficiency droop" at high input power density, which limits the number of output photons per unit area and related applications as LED for high power electricity-to-light converter systems operating at peak efficiency.[5-8] Compared with LEDs, laser diodes (LDs) do not experience "efficiency droop" above the threshold, so that high electricity-to-light conversion efficiency can be maintained at a high input power density.[9-12] Also, due to the excellent directivity of laser, the emission from LDs can be easily collected in a light beam using a lens or a mirror. For example, it is feasible to focus a 100-watt-equivalent laser light on an area as small as several millimeters in diameter.[13,14] As a result, it is widely accepted that LD-driven white lighting will be the next generation of lighting technology as a solution to the "efficiency droop" of blue LEDs.

As the input power density of the LD excitation source increases, the heat generated by the lighting device also rapidly increases.[15-18] The utilization of conventional powder phosphors in organic adhesives, with low thermal conductivity ($0.1 – 0.4$ W m^{-1} K^{-1}), requires complex cooling techniques, which critically augments the volume of the device and limits the incident power.[19,20] Moreover, non-oxide-based powder phosphors irreversibly degrade as the temperature increases, which limits their practical applications towards high-power lighting.[21] Therefore, full inorganic color converters with superior temperature characteristics can effectively improve the thermal stability of the device. There are currently three main candidates for inorganic color converter materials, *i.e.*, (i) phosphor in glass (PiG)/glass-ceramics[22], (ii) single crystals[23,-24] and (iii) transparent ceramics[25-,26]. Under high input power density, PiGs and glass-ceramics will suffer a degradation behavior during long-term operation, thus reducing the device service life and restricting their applications.[27] Single crystals

demonstrate outstanding optical and thermal properties, but their applications are limited because of low accessible chemical doping levels, restricted sizes, and high costs.[28] Also, single crystals lack tailor-made microstructures as scattering centers that play an important role in improving the excitation efficiency of the LD excitation source. On the other side, transparent ceramics are regarded as one of the most promising full inorganic color converters, given their various advantages integrating PiGs and single crystals into one, including high thermal conductivity, good mechanical properties, high doping content, microstructural flexibility, and relative cost-effectiveness.[27-31] These advantages enable transparent ceramics to match well with the requirements of LD-driven lighting systems. Recently, LD-driven lighting using transparent ceramics as color converters were reported to achieve unprecedented luminous efficiency.[32-36]

Initially, Ce^{3+}-doped $Y_3Al_5O_{12}$ garnet was considered as a possible transparent ceramic candidate for LD-driven lighting due to its successful application in white LED lighting. $Y_3Al_5O_{12}:Ce^{3+}$ ($YAG:Ce^{3+}$) transparent ceramics demonstrate good chemical stability and high quantum efficiency. However, their development remains limited due to a lack of the red-emission component and serious thermal quenching.[37,38] Recently, $Lu_3Al_5O_{12}:Ce^{3+}$ ($LuAG:Ce^{3+}$) garnet transparent ceramics have attracted more and more attention for LD lighting applications.[39] $LuAG:Ce^{3+}$ not only demonstrates strong absorption of blue light and high quantum efficiency, but also outstanding thermal stability superior to $YAG:Ce^{3+}$ due to its inherent structural rigidity and dense networked structure.[40,41] It has been reported that the luminous intensity of $LuAG:Ce^{3+}$ ceramics could remain over 90% of its initial intensity at the temperature while heated up to 450 K.[42] The emission band of $LuAG:Ce^{3+}$ is usually located in the green light region (around 520 nm), which is not suitable for white lighting under blue-emitting LD excitation. Therefore, a major challenge for using $LuAG:Ce^{3+}$ as a color converter is to broaden its emission spectrum and enhance its red emission component.

Under the circumstance of super-high power density LD lighting, another important issue is the presence of light scattering centers in transparent ceramics, which is conducive to increasing light extraction efficiency.[43] Due to the lack of scattering centers in phosphor converters, the blue laser beam will directly pass through the

phosphor material, resulting in a “yellow-ring” problem in laser lighting devices. This “yellow-ring” problem in LD-driven lighting, linked to the high directionality and focused incident source, is impeding the development of practical applications.[37] To overcome this problem and further develop LD-driven white lighting systems, external scattering centers were considered to be introduced into transparent ceramic matrices. Several strategies have been reported to disperse the extra secondary phase into phosphor ceramics, including the use of Al_2O_3[8,44], $MgAl_2O_4$[45], CaF_2[46] and AlN[47-50] particles, or even residual pores[40]. These achievements rely on the external introduction (post garnet synthesis but before sintering processing) of scattering centers in garnet-based ceramic matrices, which deteriorates densification and remains poorly dispersed.[51] To date, there is no report of a one-step approach to producing LuAG:Ce^{3+}-based transparent ceramics showing a red-shifted emission spectrum and *in situ* generated light scattering centers.

In this work, new biphasic $Lu_3MgAl_3SiO_{12}$:Ce^{3+}-based (BP-LMAS:Ce^{3+}) transparent ceramics were successfully synthesized by a multiple component design strategy that brings out both the required red-shifted emission and direct formation of a new lutetium magnesium aluminosilicate secondary phase as scattering centers. A double substitution strategy of Mg^{2+}-Si^{4+} for Al^{3+}-Al^{3+} pairs in LuAG:Ce^{3+} host is carried out to tailor the crystal field strength, leading to a drastic red-shift of the Ce^{3+} emission band to 564 nm. Meanwhile, BP-LMAS-based transparent ceramics exhibit a biphasic nested structure where the micrometer-sized *in situ* secondary phase is dispersed uniformly in the $Lu_3MgAl_3SiO_{12}$ main phase and strongly scatters the incident laser to generate highly uniform white light. An ultrahigh luminous flux of 5655 lm and low correlated color temperature of ~ 5027 K was achieved in LDs-driven white lighting under 450 nm laser excitation (laser power density 14.5 W mm^{-2}) by using BP-LMAS:0.3%Ce^{3+} transparent ceramics under a reflection mode. These results illustrate that BP-LMAS:Ce^{3+} transparent ceramics are promising candidates as color converters for high-power LDs-driven solid-state lighting.

RESULTS and DISCUSSION

Microstructure of $Lu_3MgAl_3SiO_{12}$-based transparent ceramics

$Lu_3(Mg_xAl_{5-2x}Si_x)O_{12}$-based ($x$ = 0.25–2) transparent ceramics with 0.2% Ce^{3+} doping were synthesized through solid-state reaction and subsequent hot isostatic pressing (HIP) (refer to Experimental procedures section for synthesis details). $Lu_3Al_5O_{12}$ (x = 0) transparent ceramics that are usually sintered under high vacuum conditions cannot be prepared without MgO and SiO_2 added with this process mentioned above even at the highest reaction temperature (1650 ºC). The photograph of all the prepared ceramics is shown in **Figure S1A**. The highest transmittance, 82.5% at 600 nm, is observed for x = 0.25 (1 mm thick samples) and gradually decreases for higher x values, *i.e.* Mg^{2+}-Si^{4+} content, while all samples still remain over 60% at 600 nm (**Figure S1B**). All of the prepared ceramics show high transparency and their photoluminescence (PL) spectra are given in **Figure S1C**. As x increases from 0.25 to 2, the PL peak red-shifts from 535 to 578 nm, and the full width at half maximum (FWHM) of emission band increases from 100 to 124 nm, which are ascribed to a stronger crystal field splitting effect on the 5d level of Ce^{3+} in the Mg–Si substituted aluminate garnets mentioned in previous literature[52,53]. The broadening of the emission spectrum is a crucial factor to ensure high-quality white lighting. When the Mg^{2+}-Si^{4+} contents correspond to x = 1, the emission peak is located at 558 nm, which is well suited for warm white lighting and appears more suitable than the commercial YAG:0.2%Ce^{3+} transparent ceramics (λ_{em}=535 nm, **Figure S2**). The photoluminescence excitation (PLE) spectrum of $Lu_3MgAl_3SiO_{12}$:0.2% Ce^{3+} (x = 1), monitoring the emission peak at around 558 nm (FWHM = 114 nm), exhibits two broad bands at 300–360 nm and 400–520 nm, respectively, corresponding to ultraviolet (UV) and blue light excitations. As $Lu_3MgAl_3SiO_{12}$ (x = 1) led to transparent ceramics with the optimal luminescence properties, the work presented thereafter focuses on this composition.

$Lu_3MgAl_3SiO_{12}$-based transparent ceramics were elaborated by precisely controlling the solid-reaction sintering process prior to HIP for enabling *in situ* formation of a secondary phase. **Figure 1A** shows the backscattered electron image of the mirror-polished surface of $Lu_3MgAl_3SiO_{12}$-based transparent ceramics. The sample

appears very dense with no obvious porosity and composed of a grey major phase with a brighter secondary phase which is uniformly dispersed at the grain boundaries of the major phase. The average grain size of the major phase is about 3.85 μm (+/-0.05 μm) and larger than the secondary phase (1.65 μm+/-0.05 μm). By image analysis on SEM micrographs, the volume fraction of the secondary phase was estimated as 2.5% vol. (+/-0.5%). Elemental mapping images of energy-dispersive X-ray spectroscopy (EDS) (**Figure 1 B–E**) illustrates the presence of two different phases with differences in element composition. Quantitative EDS analysis (**Figure S3**) confirms that the composition of the major phase matches to a LuAG garnet material with equimolar Mg and Si elements substituting for Al, *i.e.* $Lu_3MgAl_3SiO_{12}$. The secondary phase appears richer in Lu and deficient in Mg and Al in comparison with the major phase. Its average composition could not be attributed to any known phase. The results of electron probe micro-analysis (EPMA) prove the element ratio of the $Lu_3MgAl_3SiO_{12}$-based transparent ceramic in relatively good agreement with the initial formula $Lu_3MgAl_3SiO_{12}$ (**Figure S4**). Therefore, elemental volatilization was not detected on the sample.

Rietveld refinement analysis of the XRPD data from biphasic $Lu_3MgAl_3SiO_{12}$ (BP-LMAS) transparent ceramics was performed, as shown in **Figure 1F**. The main peaks are consistent with the patterns of $Lu_3Al_5O_{12}$ garnet phase (PDF#73-1368) despite a slight shift, supporting the deduction that the major phase is the garnet-structured solid solution of $Lu_3MgAl_3SiO_{12}$ phase. The unit cell parameter was refined as a = 11.95590(1) Å, which is larger than that of $Lu_3Al_5O_{12}$ phase (*i.e.*, 11.9181 Å).[52,54] It is reasonable to deduce that the larger cell volume is ascribed to the double substitution of Mg^{2+}-Si^{4+} pairs for Al^{3+}-Al^{3+} pairs in LuAG.[52,53,55] The atom coordinates and main bond lengths obtained from the Rietveld refinement are shown in **Tables S1** and **Table S2**. Final refinement of this model with low R-factors was stable with low R-factors (GOF = 5.2, Rp = 4.03%, Rwp = 5.81%). In coupling these results with diffraction data, we could determine that the secondary phase is a $Lu_4Al_2O_9$-based material in which Mg and Si respectively substitute to Lu and Al (composition close to $Lu_{3.5}Mg_{0.5}Al_{1.5}Si_{0.5}O_9$,), and the nominal chemical formula of the new phase is

$(Lu/Mg)_4(Al/Si)_2O_9$. The amount of the $(Lu/Mg)_4(Al/Si)_2O_9$ secondary phase was refined as 3.6(1) wt.% (*i.e.* 3.2(1) vol.%) according to Rietveld refinement results, in good agreement with SEM observations. The structure and optical properties of this new $(Lu/Mg)_4(Al/Si)_2O_9$ material are currently under study.

To gain more (micro)structural information on the BP-LMAS transparent ceramic, high resolution transmission electron microscopy (HRTEM) imaging was engaged. **Figure 1G** shows a typical grain boundary between the garnet phase $Lu_3MgAl_3SiO_{12}$ and the secondary phase $(Lu/Mg)_4(Al/Si)_2O_9$. The boundary is rather thin (*c.a.* 3 nm) and homogenous without any residual porosity or elemental segregation. The major phase crystal lattice was confirmed to be garnet phase by Fourier transform electron diffraction, as shown in the inset. The cationic components of the secondary phase analyzed by STEM–EDS (**Figures 1H and I**), shows that the secondary phase is $(Lu/Mg)_4(Al/Si)_2O_9$, *i.e.* enriched in Lu and Si compared to the garnet phase, which is consistent with the above SEM-EDS results.

Evolution of the $(Lu/Mg)_4(Al/Si)_2O_9$ phase with sintering temperature

The *in situ* formation of the $(Lu/Mg)_4(Al/Si)_2O_9$ secondary phase can be effectively controlled by simply regulating the solid reaction sintering temperature. Sintering of $Lu_3MgAl_3SiO_{12}$-based transparent ceramics was conducted at 1550–1650 ^oC. The XPRD results indicate that the secondary phase gradually disappeared with sintering temperature increasing (**Figure 2A**), and a high sintering temperature is beneficial to obtain better transparency, as displayed in the inset. The SEM images of $Lu_3MgAl_3SiO_{12}$ transparent ceramics prepared at varying temperatures, are presented in **Figure S5**. The secondary phase merely appears at sintering temperatures of 1550–1625 ^oC, and disappears at 1650 ^oC. The evolution of the micrograph of the secondary phase is in accordance with the XRPD analysis. A similar phase evolution was observed in $Lu_{2.94}Ce_{0.06}Mg_2Al_{3-x}Si_xO_{12}$ (x = 0–2) phosphors.[59] **Figure 2B** demonstrates the optical transmittance of transparent ceramics that were sintered at different temperatures prior to HIP process. The $Lu_3MgAl_3SiO_{12}$ transparent ceramics sintered at 1650 ^oC exhibit a transmittance as high as 77.3% at 600 nm (1 mm thickness). Owing to the scattering effect of the secondary phase, BP-LMAS transparent ceramics sintered

at 1625 ºC show a lower transmittance (62.9% at 600 nm), and the other ceramics sintered at 1550 and 1600 ºC are nearly opaque. The SEM images of transparent ceramics that were sintered at different temperatures after HIP process are free of pores, indicative of full densification (**Figure 2C-F**). Therefore, HIP treatment with 1600 ºC and 200 MPa condition is an effective means of eliminating residual porosity when the ceramic has been sintered at 1625 ºC, however, it has no impact on inhibiting the formation of the secondary phase.

Luminescence properties of BP-LMAS:Ce^{3+} transparent ceramics

The PL spectra of the BP-LMAS:*y*Ce^{3+} (*y* = 0.1–1.5%) transparent ceramics doped with different Ce^{3+} concentrations are displayed **Figure 3A**. The highest PL intensity can be reached at *y* = 0.3%, and the emission maximum is redshifted from 552 to 568 nm with *y* increasing from 0.1 to 1.5% (**Figure S6A**). The inset of **Figure 3B** shows photographs of BP-LMAS:*y*Ce^{3+} transparent ceramics with a thickness of 1.0 mm, and their optical transmittance spectra are presented in **Figure S6B**. For Ce^{3+} doping concentration up to 0.5% or higher, the transmittance does not change near 450 nm, which correspond to the integrated absorption of Ce^{3+} reaching saturation, indicating that the optimal Ce^{3+} content can be a lower concentration (*y* = 0.3%). Accordingly, it also shows the maximal internal/external quantum efficiency (IQE/EQE) of 76.1/65.2% under 450 nm excitation (**Figure 3B**), which even better than the reported $Lu_3MgAl_3SiO_{12}$:0.06Ce^{3+} phosphors with IQE/EQE of 69.1/44.9%.[53] The PLE and PL spectra of LuAG:0.3%Ce^{3+} and BP-LMAS:0.3%Ce^{3+} transparent ceramics are presented in **Figure 3C**. The two broad excitation bands located at about 340 and 450 nm are attributed to the electronic transitions of Ce^{3+} form $4f^1$ to $5d^2$ and $5d^1$ excited energy levels, respectively. The opposite shift of the two excitation peaks and the broadening of excitation bands are affected by the host composition. It was reported that the substitution of Mg^{2+}-Si^{4+} pairs for Al^{3+}-Al^{3+} increased the distortion of the dodecahedron (CeO_8),[55,57] leading to the diversified coordination environment of Ce^{3+}, which in turn contributes to the broadening of PLE and PL spectra. Correspondingly, a red-shift emission of Ce^{3+} occurs, which is ascribed to the changeable nephelauxetic effect, crystal-field splitting, and Stokes shift. (**Figure S7**). The emission peak shifts

from a green light region (λ_{em} = 520 nm) for LuAG:0.3%Ce^{3+} to a yellow-orange light region (λ_{em} = 564 nm) for BP-LMAS:0.3%Ce^{3+}, which enables the BP-LMAS:0.3%Ce^{3+} transparent ceramic to be used for warm white lighting applications. Moreover, FWHM of BP-LMAS:0.3%Ce^{3+} (114 nm) is larger than LuAG:0.3%Ce^{3+} (~ 90 nm). Moreover, displayed in **Figure 3D**, BP-LMAS:0.3%Ce^{3+} also exhibits a shorter average lifetime (55.3 ns) compared to that of LuAG:0.3%Ce^{3+} (58.5 ns), indicating that the non-thermal optical saturation can be reduced under high-power density excitation.[58] Ce^{3+} ions are located in distinct coordination environments due to the formation of Si^{4+}- and Mg^{2+}-rich local region, causing the energy transfer process and stronger emission reabsorption to takes place, which shorten the fluorescence lifetime.

Thermal stability is crucial for luminescent materials used in LDs driven lighting. As seen in **Figure 3E**, the IQE and EQE values of the BP-LMAS:0.3%Ce^{3+} transparent ceramic decrease by only 8% when the temperature increases from room temperature (RT) to 423 K, which is much lower than for YAG:Ce phosphors (15% decrease).[38] **Figure 3F** displays a contour plot of thermal quenching behaviors of BP-LMAS:0.3%Ce^{3+} transparent ceramic under 450 nm excitation at a temperature range of 298 – 473 K with an interval of 25 K. Heated up to 423 K, the emission intensity remains 93.1% of its value at RT. The temperature dependence properties of LuAG: 0.3%Ce^{3+} are given in **Figure S8**. With the temperature up to 473 K, the relative integrated emission intensity of LuAG:0.3% Ce^{3+} remains at about 97.3% of its value at RT. The thermal stability decreases with Mg^{2+}-Si^{4+} substitution due to the narrowed band gap of the host and the enhanced crystal field splitting of Ce^{3+}, which reduces the energy difference between the conduction band bottom and the 5d levels of Ce^{3+}, and the thermal activation energy becomes lower. Chromaticity stability is also an important parameter of thermal stability of luminescence. The CIE color coordinates of the BP-LMAS:0.3% Ce^{3+} slightly shift to the red region with the temperature increasing from 298 to 473 K (**Figure S9**). The chromaticity stability is also better than that of YAG:0.5% Ce,0.02% Mg,0.02% Si[13]. Regarding the LMAS:0.3% Ce^{3+} transparent ceramic, the thermal conductivity can be measured by the transient plane source method. The thermal conductivity of LMAS:0.3% Ce^{3+} transparent ceramics is 3.57 $W \cdot m^{-1} \cdot K^{-1}$ at

25 °C, *i.e.* slightly lower than for LuAG:0.3% Ce^{3+} transparent ceramics (4.36 $W \cdot m^{-1} \cdot K^{-1}$) but much higher than phosphor glasses (<1 $W \cdot m^{-1} \cdot K^{-1}$).[10,11] The above results imply that the BP-LMAS:0.3% Ce^{3+} transparent ceramic is thermally robust for use in high-power LD-driven lighting.

Evaluation of light scattering in the BP-LMAS:0.3% Ce^{3+} transparent ceramic

The light scattering properties of LuAG:0.3% Ce^{3+} and BP-LMAS:0.3% Ce^{3+} transparent ceramics were investigated by using laser scanning confocal imaging (**Figures 4A** and **B**). Under 470 nm laser irradiation, both samples show different luminous surfaces, and the brighter the color, the higher the luminous intensity. Owing to the presence of the secondary phase in BP-LMAS:0.3% Ce^{3+}, the blue light beam can be adequately absorbed and mixed, resulting in a more uniform luminous surface, also demonstrated by the 3D images of **Figures S10A and B,** respectively. The luminescence intensities are different between the grain interior and the grain boundary of LuAG:0.3% Ce^{3+} transparent ceramics. The role of the secondary phase as scattering centers was proved based on the comparison of the transmittance data recorded with two different measurement modes. However, the amount of secondary phase is limited, and does not influence the luminescence intensity and wavelength of BP-LMAS:0.3% Ce^{3+}. The schematic diagrams of in-line and integrating sphere measurements are presented in **Figures S11A and B**, respectively, and the transmittance spectra are illustrated in **Figure 4C**. The transmittance of BP-LMAS:0.3% Ce^{3+} is reduced from 76% (integrating sphere detector) to 41% (in-line detector) at 600 nm, correspondingly, it just decreases from 82% to 62% for LuAG:0.3% Ce^{3+}, and the transmittance of single-phase (SP) LMAS:0.3% Ce^{3+} transparent ceramics also decreases from 79% to 57%. The remarkable decrease of transmittance in BP-LMAS:0.3% Ce^{3+} is ascribed to the effective light scattering by the secondary phase, alike to the phenomenon detected in phosphor-in-glass materials where the transmittance declines along with the increase of the phosphor content.[59] The size of the secondary phase grains is micron scale in our material, therefore much larger than the incident visible wavelength. In this case, the Mie scattering theory[60-62] can be applied. Note that if the size of the grains would have been very small, especially compared to the size of the incident wavelength, then

Rayleigh scattering would have occurred and limited scattering effect would have taken place. In our case the scattering effect is large, because the refractive index of the non-cubic secondary phase is different from that of the major phase. Therefore, the secondary phase plays a significant role in enhancing the total light output by multiple scattering of the incident blue light to improve conversion efficiency. LD-driven lighting images are obtained by pumping the two ceramics with a 4.35 W blue LD (**Figures 4D and E**). An obvious blue spot can be seen for LuAG:0.3% Ce^{3+}, which is ascribed to the directly transmitted blue light from the LD. In comparison, BP-LMAS:0.3% Ce^{3+} demonstrates an effective solution for overcoming the "yellow-ring" problem of the LD-driven white lighting[63,64], schematic illustration as **Figure 4F** presented.

Demonstration of LDs-driven lighting

Figure S12A presents the schematic diagram and photographs of the LD-driven lighting test system, and a scheme of the light path of the transmission mode is shown in **Figure S12B**. For LD-driven white lighting, the thickness of the phosphor material plays a significant role in producing uniform white lighting. **Figure 5A** exposes the output luminous flux of BP-LMAS:0.3% Ce^{3+} transparent ceramics with varying thicknesses as a function of the incident power, measured in a transmission mode. The BP-LMAS:0.3% Ce^{3+} transparent ceramic with a thickness of 1.2 mm shows the highest luminous flux of 2725 lm under blue laser excitation with a power density of 17.3 W mm^{-2}. Electroluminescence (EL) spectra of the BP-LMAS:0.3% Ce^{3+} transparent ceramics with a thickness ranging from 0.2 to 1.2 mm, under 11.4 W mm^{-2} laser excitation, were measured in a transmission mode (**Figure 5B)**. It shows that LD-driven white lighting in transmission mode usually requires a thicker transparent ceramic to ensure adequate absorption of the incident blue-emitting laser, and to make output light more uniform.

To improve the safety of laser lighting and heat dissipation of phosphors, LD-driven white lighting in a reflection mode is brought into focus, the light path of which is depicted in **Figure S12C**. As displayed in **Figure 5C**, the color coordinates of the emitted light in a reflection mode shift from blue-green to white, and then eventually to

the orange-yellow region with increasing the thickness. The BP-LMAS:0.3% Ce^{3+} transparent ceramic with a thickness of 0.4 mm enables chromaticity coordinates of (0.3444, 0.3530) with the luminous efficacy of 130 lm W^{-1} and the white light correlated color temperature (CCT) of 5027 K. In this case, the ceramic can effectively scatter and absorb the highly directional laser to generate the uniform white lighting. With increasing the input electric power up to 144 W, the luminous flux of the ceramic does not decrease yet (**Figure 5D**). The highest luminous flux can reach 5655 lm when the power density is 14.5 W mm^{-2}, and the spot size is 1 × 3 mm^2. The photochromic properties of the BP-LMAS:0.3%Ce^{3+} transparent ceramics, measured in both transmission and reflection modes, are given in **Tables S3 and S4**. It is easier to achieve a high power density in reflection mode than transmission mode, due to faster dissipation of the waste heat (produced by luminescence from the ceramic) by the heat sink. For long distance lighting, the reflection mode is preferred as it promises better heat dissipation and higher luminous flux. As demonstrated in **Figure S13**, the LD-driven white lighting in reflection mode can easily irradiate at a distance longer than 1000 m.

In summary, we have successfully prepared a series of $Lu_3(Mg_xAl_{5-2x}Si_x)O_{12}:Ce^{3+}$ (x = 0.25–2) transparent ceramics, which enlarge the garnet-based transparent ceramic family. Amongst, the BP-LMAS:0.3% Ce^{3+} (x = 1) transparent ceramics demonstrate a broad yellow-orange emission (λ_{em} = 564 nm, FWHM=114 nm), with a $(Lu/Mg)_4(Al/Si)_2O_9$ secondary phase (3.2(1) vol.%) formed *in-situ* providing scattering centers that play an important role in scattering of the incident laser beam. The sintering temperature has been regulated to control the presence or absence of secondary phase, and the SP $Lu_3MgAl_3SiO_{12}$ transparent ceramics can be obtained sintered at 1650 °C. The BP-LMAS:0.3% Ce^{3+} transparent ceramic, having a high transmittance of 76%@600 nm and quantum efficiency of 76.1%, allows to produce uniform LD-driven white lighting. We expect the biphasic ceramics with secondary phases formed *in-situ* will achieve final industrial applications in high-power lighting.

EXPERIMENTAL PROCEDURES

Resource availability

Lead contact

Further information and requests for resources should be directed to and will be fulfilled by the lead contact, Jianqiang Li (jianqiangli@ustb.edu.cn).

Materials availability

The materials described in this study can be made available upon request.

Data and code availability

Data reported in this paper are available from the lead contact upon reasonable request. No new code was developed in this study.

Transparent Ceramics Preparation

$Lu_3(Mg_xAl_{5-2x}Si_x)O_{12}$ (x = 0.25–2) and BP-LMAS:$y$$Ce^{3+}$ (y = 0.1%, 0.3%, 0.5%, 1.0% and 1.5%, with substitution of Ce^{3+} for Lu^{3+}) transparent ceramics were prepared by solid state reaction. The raw materials, including high purity commercial Al_2O_3 (99.99%, Taimei Chemistry Co., Ltd, Japan), Lu_2O_3 (99.99%, Rare-chem Hi-tach Co., Ltd, China), $MgCO_3$, SiO_2, and CeO_2 (99.99%, Beijing Dk Nano technology Co., Ltd, China) were weighted in stoichiometric ratios and homogeneously mixed and milled for 12 h in ethanol. The powder mixtures were dried at 60 ºC in an oven for 12 hours to remove the ethanol solvent. After being ground and sieved through a 200-mesh screen, the powder mixtures were calcined at 900 ºC for 2 h in air. The calcined powders were uniaxially pressed into pellets (Φ = 15 mm) in a steel mold at 1.5 MPa pressure and then subjected to cold isostatic pressing at 200 MPa. The pellets were sintered at 1550 – 1650 ºC in a high-temperature muffle furnace followed by hot isostatic pressing at 1600 ºC for 2h, and then annealed in air at 1100–1300 ºC for 6 h. $Lu_3Al_5O_{12}$:Ce^{3+} transparent ceramics were prepared by the same process except for the sintering method of high vacuum at 1800 ºC for 10 h. Subsequently, all the ceramics were polished on

both sides for optical characterization, and then polished to different thicknesses (0.2 mm, 0.4 mm, 0.8 mm, and 1.2 mm) for further structural and optical characterizations.

Microstructure analysis

The micromorphology and cathode ray luminescence spectra of the ceramics were characterized by field emission scanning electron microscope (SEM, Quanta 250, FEI, USA) and energy dispersive X-ray spectroscopy (EDS) was employed to measure the elemental composition. The area fraction of the secondary phase was quantified by analyzing SEM images recorded in back scattering electron mode, and the volume fraction of the secondary phase is estimated from SEM images using the ImageJ software (https://imagej.nih.gov/ij/index.html). Binary images of the secondary phase were obtained after thresholding and removing isolated pixels using an OPEN filter. Electron probe micro-analysis (EPMA, SS94000, JEOL, Japan) was adopted to analyze element ratio of this BP-LMAS:0.3% Ce^{3+} transparent ceramics. XRPD patterns data were collected using a diffractometer (Bruker D8 Advance Bruker, Karlsruhe, Germany) operating at 40 kV and 40 mA with monochromatized Cu-Kα radiation (λ = 1.5406 Å). High-resolution TEM and STEM-EDS micrographs of the different phases and their boundary, as well as corresponding elemental information were acquired using a Cold FEG Transmission Electron Microscope (TEM, ARM 200F, JEOL, Japan) operating at 200 kV, equipped with a double spherical corrector and fitted with a JEOL SDD CENTURIO EDS system. The thermal conductivity of transparent ceramics was measured by Hot Disk heat conductivity meter (Hot Disk, TPS2500s, Sweden).

Luminescence properties tests

Transmittance was recorded on double-mirror polished samples using a UV–VIS spectrophotometer (Cary 7000, Aligent Technologies, USA) with air as a reference. The PL and PLE spectra were measured at room temperature with a FL-111 fluorescence spectrophotometer (HORIBA, Japan) using a Xe-900 lamp as the excitation source. The absorption, internal and external quantum efficiency values were measured using the integrated sphere on the QE-2100 spectrophotometer from Otsuka Photal Electronics, and white $BaSO_4$ powder was used as a reference to measure the absorption. The decay curves were measured with the same instrument using a flash lamp as the excitation

source. The temperature-dependent spectra from 298 K to 473 K were obtained by a heating apparatus attached to the FL3-111 spectrophotometer. The scattering effect of secondary phases was assessed by a confocal laser scanning microscope (CLSM, Leica SP8 STED 3X, Leica Micromanipulator, Germany) where the sample was excited by a 450 nm argon laser and the image was acquired in confocal mode.

LD-Driven Lighting Fabrication and Measure

This system consists of high-power blue laser sources and an integrating sphere (PMS-50, Everfine, China), which is connected to a multichannel spectrometer (F-4600, Hitachi, Japan). High-power blue laser sources consist of 10 blue laser diodes (λ_{em} = 450 nm, NICHIA, Japan), which were focused into a minimum spot of 1 mm diameter by a condenser lens. The optical power of the laser diodes was stabilized by a thermoelectric cooler module setting at 25 ^{o}C. Commission Internationale de l'Eclairage (CIE) chromaticity coordinate, correlated color temperature (CCT), and luminous flux were measured by using an integrating sphere under the 450 nm laser excitation. The transparent ceramics were excited and measured by blue LDs under transmission and reflection modes, respectively.

SUPPLEMENTAL INFORMATION

Supplemental information can be found online.

ACKNOWLEDGMENTS

This work is financially supported by the National Natural Science Foundation of China (NSFC No. 51972304, No. 51971208), Beijing Municipal Science and Technology Project (No. Z191100004819002), the Project of Scientific Experiment on Chinese Manned Space Station, key research and development project of Jiangxi Province (20212BBE53050) and the Fundamental Research Funds for the Central Universities. The authors acknowledge the financial support by the ANR-18-CE08-0012 PERSIST project of the French National Research Agency. This project has benefited from the facilities of the Platform MACLE-CVL which was co-funded by the European Union

and Centre-Val de Loire Region (FEDER). The authors acknowledge M.P. Chauvat and P. Ruterana from the CIMAP laboratory (Caen, France) for the sample preparation by PIPS II.

AUTHOR CONTRIBUTIONS

M. A., H. Q. and J. L. oversaw all research; S. F. designed the experiments; Y. G., J. F., C. G., and E. V. performed the microstructure test and data analysis; H. W. and Y. Y. analyzed and interpreted the data of microstructure; S. L. and R-J. X. provided expertise and feedback; S. F. performed the luminescence properties measurements and data analysis; S. F., M. A., H. Q. and J. L. wrote and revised the manuscript; all authors reviewed and edited the manuscript.

DECLARATION OF INTERESTS

All authors declare no competing financial interest.

REFERENCES

1. Schubert, E.F., and Kim, J.K. (2005). Solid-state light sources getting smart. Science *308*, 1274-1278.
2. Pimputkar, S., Speck, J.S., DenBaars, S.P., and Nakamura, S. (2009). Prospects for LED lighting. Nat. Photon. *3*, 179-181.
3. Pust, P., Schmidt, P.J., and Schnick, W. (2015). A revolution in lighting. Nat. Mater. *14*, 454-458.
4. Zhao, M., Liao, H., Molokeev, M.S., Zhou, Y., Zhang, Q., Liu, Q., and Xia, Z. (2019). Emerging ultra-narrow-band cyan-emitting phosphor for white LEDs with enhanced color rendition. Light: Sci. Appl. *8*, 38.
5. Neumann, A., Wierer, J.J., Davis, W., Ohno, Y., Brueck, S.R.J., and Tsao, J.Y. (2011). Four-color laser white illuminant demonstrating high color-rendering quality. Opt. Express *19*, A982-A990.
6. Wierer, J.J., Tsao, J.Y., and Sizov, D.S. (2013). Comparison between blue lasers and light-emitting diodes for future solid-state lighting. Laser Photonics Rev. *7*, 963-993.

7. Kane, M.H., Jiao, J., Dietz, N., Huang, J.-J., Lenef, A., Kelso, J., Tchoul, M., Mehl, O., Sorg, J., and Zheng, Y. (2014). Laser-activated remote phosphor conversion with ceramic phosphors. 13th International Conference on Solid State Lighting *9190*, 91900C.
8. Li, S., Zhu, Q., Tang, D., Liu, X., Ouyang, G., Cao, L., Hirosaki, N., Nishimura, T., Huang, Z., and Xie, R.-J. (2016). Al_2O_3-YAG:Ce composite phosphor ceramic: a thermally robust and efficient color converter for solid state laser lighting. J. Mater. Chem. C *4*, 8648-8654.
9. You, S., Li, S., Zheng, P., Zhou, T., Wang, L., Liu, L., Horisaki, N., Xu, F., and Xie, R.-J. (2019). A Thermally Robust $La_3Si_6N_{11}$:Ce-in-Glass Film for High-Brightness Blue-Laser-Driven Solid State Lighting. Laser Photonics Rev. *13*, 1800216.
10. Zhang, X., Yu, J., Wang, J., Lei, B., Liu, Y., Cho, Y., Xie, R.-J., Zhang, H.-W., Li, Y., Tian, Z., Li, Y., and Su, Q. (2017). All-Inorganic Light Convertor Based on Phosphor-in-Glass Engineering for Next-Generation Modular High-Brightness White LEDs/LDs. ACS Photonics *4*, 986-995.
11. Zheng, P., Li, S., Wang, L., Zhou, T.L., You, S., Takeda, T., Hirosaki, N., and Xie, R.J. (2018). Unique Color Converter Architecture Enabling Phosphor-in-Glass (PiG) Films Suitable for High-Power and High-Luminance Laser-Driven White Lighting. ACS Appl. Mater. Interfaces *10*, 14930-14940.
12. Strek, W., Cichy, B., Radosinski, L., Gluchowski, P., Marciniak, L., Lukaszewicz, M., and Hreniak, D. (2015). Laser-induced white-light emission from graphene ceramics–opening a band gap in graphene. Light: Sci. Appl. 4, e237.
13. Yao, Q., Hu, P., Sun, P., Liu, M., Dong, R., Chao, K., Liu, Y., Jiang, J., and Jiang, H. (2020). YAG:Ce^{3+} Transparent Ceramic Phosphors Brighten the Next-Generation Laser-Driven Lighting. Adv. Mater. *32*, e1907888.
14. Xu, Y., Li, S., Zheng, P., Wang, L., You, S., Takeda, T., Hirosaki, N., and Xie, R.-J. (2019). A search for extra-high brightness laser-driven color converters by investigating thermally-induced luminance saturation. J. Mater. Chem. C *7*, 11449-11456.
15. Kim, Y.H., Arunkumar, P., Kim, B.Y., Unithrattil, S., Kim, E., Moon, S.H., Hyun, J.Y., Kim, K.H., Lee, D., Lee, J.S., and Im, W. B. (2017). A zero-thermal-quenching phosphor. Nat. Mater. *16*, 543-550.
16. Park, J., Cho, S., and Kwon, H. (2018). Aluminum-ceramic composites for thermal management in energy-conversion systems. Sci. Rep. *8*, 17852.
17. Ma, Y., Lan, W., Xie, B., Hu, R., and Luo, X. (2018). An optical-thermal model for laser-excited remote phosphor with thermal quenching. Inter. J. Heat and Mass Transfer *116*, 694-702.
18. Kim, E., Shim, H.W., Unithrattil, S., Kim, Y.H., Choi, H., Ahn, K.J., Kwak, J.S., Kim, S., Yoon, H., and Im, W.B. (2016). Effective Heat Dissipation from Color-Converting Plates in High-Power White Light Emitting Diodes by Transparent Graphene Wrapping. ACS Nano *10*, 238-245.
19. Yu, J., Si, S., Liu, Y., Zhang, X., Cho, Y., Tian, Z., Xie, R.-J., Zhang, H., Li, Y., and Wang, J. (2018). High-power laser-driven phosphor-in-glass for

excellently high conversion efficiency white light generation for special illumination or display backlighting. J. Mater. Chem. C *6*, 8212-8218.
20. Zhang, X., Si, S., Yu, J., Wang, Z., Zhang, R., Lei, B., Liu, Y., Zhuang, J., Hu, C., Cho, Y., Xie, R.-J., Zhang, H., Tian, Z. and Wang, J. (2019). Improving the luminous efficacy and resistance to blue laser irradiation of phosphor-in-glass based solid state laser lighting through employing dual-functional sapphire plate. J. Mater. Chem. C *7*, 354-361.
21. Zhu, Q.-Q., Wang, X.-J., Wang, L., Hirosaki, N., Nishimura, T., Tian, Z.-F., Li, Q., Xu, Y.-Z., Xu, X., and Xie, R.-J. (2015). beta-Sialon:Eu phosphor-in-glass: a robust green color converter for high power blue laser lighting. Journal of Materials Chemistry C *3*, 10761-10766.
22. Lin, H., Hu, T., Cheng, Y., Chen, M., and Wang, Y. (2018). Glass Ceramic Phosphors: Towards Long-Lifetime High-Power White Light-Emitting-Diode Applications-A Review. Laser Photonics Rev. *12*, 1700344.
23. Balci, M.H., Chen, F., Cunbul, A.B., Svensen, Akram, M.N., and Chen, X. (2017). Comparative study of blue laser diode driven cerium-doped single crystal phosphors in application of high-power lighting and display technologies. Opt. Rev. *25*, 166-174.
24. Xu, J., Thorseth, A., Xu, C., Krasnoshchoka, A., Rosendal, M., Dam-Hansen, C., Du, B., Gong, Y., and Jensen, O.B. (2019). Investigation of laser-induced luminescence saturation in a single-crystal YAG:Ce phosphor: Towards unique architecture, high saturation threshold, and high-brightness laser-driven white lighting. J. Lumin. *212*, 279-285.
25. Ma, X., Li, X., Li, J., Genevois, C., Ma, B., Etienne, A., Wan, C., Veron, E., Peng, Z., and Allix, M. (2018). Pressureless glass crystallization of transparent yttrium aluminum garnet-based nanoceramics. Nat. Commun. *9*, 1175.
26. Yuan, Y., Wang, D., Zhou, B., Feng, S., Sun, M., Zhang, S., Gao, W., Bi, Y., and Qin, H. (2018). High luminous fluorescence generation using Ce:YAG transparent ceramic excited by blue laser diode. Opt. Mater. Express *8*, 2760.
27. Li, S., Wang, L., Hirosaki, N., and Xie, R.-J. (2018). Color Conversion Materials for High-Brightness Laser-Driven Solid-State Lighting. Laser Photonics Rev. *12*, 1800173.
28. Ma C.Y., and Cao, Y.G. (2021) Phosphor converters for laser driven light sources. Appl. Phys. Lett. *118*, 210503.
29. Lin, J.F., Zhou, Y., Lu, Q.L., Wu, X., Lin, C., Lin, T.F, Xue, K.-H., Miao, X.S., Sa, B.S., and Sun, Z.M. Reversible modulation of photoenergy in Sm-doped $(K_{0.5}Na_{0.5})NbO_3$ transparent ceramics via photochromic behavior. (2019). J. Mater. Chem. A *7*, 19374-19384.
30. Wu, X., Lin, J.F., Xu, Z., Zhao, C..L., Lin, C., Wang, H.J., Lin, T.F., Zheng, X.H., Sa, B.S., Zhang, Q.W., Wang, K., Sun, Z.M., and Zhai, J.W. (2021). Defect management and multi-mode optoelectronic manipulations *via* photo-thermochromism in smart windows. Laser Photonics Rev. *15*, 2100211.
31. Wang, Z., Zhou, G., Jiang, D., and Wang, S. (2018). Recent development of $A_2B_2O_7$ system transparent ceramics. J. Adv. Ceram. *7*, 289-306.

32. Kang, J., Zhang, L., Li, Y., Ma, Y., Sun, B., Liu, Y., Zhou, T., Selim, F.A., Wong, C., and Chen, H. (2019). Luminescence declining behaviors in YAG:Ce transparent ceramics for high power laser lighting. J. Mater. Chem. C *7*, 14357-14365.
33. Liu, X., Zhou, H., Hu, Z., Chen, X., Shi, Y., Zou, J., and Li, J. (2019). Transparent Ce:GdYAG ceramic color converters for high-brightness white LEDs and LDs. Opt. Mater. *88*, 97-102.
34. Sun, B., Zhang, L., Zhou, T., Shao, C., Zhang, L., Ma, Y., Yao, Q., Jiang, Z., Selim, F.A., and Chen, H. (2019). Protected-annealing regulated defects to improve optical properties and luminescence performance of Ce:YAG transparent ceramics for white LEDs. J. Mater. Chem. C *7*, 4057-4065.
35. Hua, H., Feng, S., Ouyang, Z., Shao, H., Qin, H., Ding, H., Du, Q., Zhang, Z., Jiang, J., and Jiang, H. (2019). YAGG:Ce transparent ceramics with high luminous efficiency for solid-state lighting application. J. Adv. Ceram. *8*, 389-398.
36. Feng, S., Qin, H., Wu, G., Jiang, H., Zhao, J., Liu, Y., Luo, Z., Qiao, J., and Jiang, J. (2017). Spectrum regulation of YAG:Ce transparent ceramics with Pr, Cr doping for white light emitting diodes application. J. Eur. Ceram. Soc. *37*, 3403-3409.
37. Anant A. Setlur, Heward, W.J., Gao, Y., Srivastava, A.M., Chandran, R.G., and Shankar, M.V. (2006). Crystal Chemistry and Luminescence of Ce^{3+}-Doped $Lu_2CaMg_2(Si,Ge)_3O_{12}$ and Its Use in LED Based Lighting. Chem. Mater. *18*, 3314-3322.
38. Bachmann, V., Ronda, C., and Meijerink, A. (2009). Temperature Quenching of Yellow Ce^{3+} Luminescence in YAG:Ce. Chem. Mater. *21*, 2077–2084.
39. Li, K., Shi, Y., Jia, F., Price, C., Gong, Y., Huang, J., Copner, N., Cao, H., Yang, L., Chen, S., Chen, H., and Li, J. (2018). Low Etendue Yellow-Green Solid-State Light Generation by Laser-Pumped LuAG:Ce Ceramic. IEEE Photonics Tech. Letters *30*, 939-942.
40. Zhang, Y., Hu, S., Wang, Z., Zhou, G., and Wang, S. (2018). Pore-existing $Lu_3Al_5O_{12}$:Ce ceramic phosphor: An efficient green color converter for laser light source. J. Lumin. *197*, 331-334.
41. Xu, J., Wang, J., Gong, Y., Ruan, X., Liu, Z., Hu, B., Liu, B., Li, H., Wang, X., and Du, B. (2018). Investigation of an LuAG:Ce translucent ceramic synthesized via spark plasma sintering: Towards a facile synthetic route, robust thermal performance, and high-power solid state laser lighting. J. Euro. Ceram. Soc. *38*, 343-347.
42. Chen, L., Lin, C.-C., Yeh, C.-W., and Liu, R.-S. (2010). Light Converting Inorganic Phosphors for White Light-Emitting Diodes. Materials *3*, 2172-2195.
43. Zhou, Y., Yu, C., Song, E., Wang, Y., Ming, H., Xia, Z., and Zhang, Q. (2020). Three Birds with One Stone: $K_2SiF_6:Mn^{4+}$ Single Crystal Phosphors for High-Power and Laser-Driven Lighting. Adv. Optical Mater. *8*, 2000976.
44. Liu, Z., Li, S., Huang, Y., Wang, L., Zhang, H., Jiang, R., Huang, F., Yao, X.,

Liu, X., and Huang, Z. (2019). The effect of the porosity on the Al_2O_3-YAG:Ce phosphor ceramic: Microstructure, luminescent efficiency, and luminous stability in laser-driven lighting. J. Alloys and Comp. *785*, 125-130.

45. Liu, X., Qian, X., Zheng, P., Hu, Z., Chen, X., Pan, H., Zou, J., Xie, R.-J., and Li, J. (2019). Preparation and optical properties of $MgAl_2O_4$-Ce:GdYAG composite ceramic phosphors for white LEDs. J. Euro. Ceram. Soc. *39*, 4965-4971.
46. Gu, C., Wang, X.-J., Xia, C., Li, S., Liu, P., Li, D., Li, H., Zhou, G., Zhang, J., and Xie, R.-J. (2019). A new CaF_2-YAG:Ce composite phosphor ceramic for high-power and high-color-rendering WLEDs. J. Mater. Chem. C *7*, 8569-8574.
47. Peng, X.L, Li, S.X, Liu, Z.H., Zhang, B.H., Peng, Y.S., Yu, D., Tian, R.D., Yao, X.M., Huang, Z.R., Liu, and X.J., Xie, R.-J. (2021). Highly thermal conductive red-emitting AlN-$CaAlSiN_3$:Eu^{2+} composite phosphor ceramics for high-power laser-driven lighting. J. Eur. Ceram. Soc. *41*, 5650-5657.
48. Fujioka, K., Yagasaki, K., Sawada, T., Minemoto, H., Fuji, H., and Yamamoto, K. (2021). AlN–Ce-doped yttrium aluminum garnet composite ceramic phosphor for high-power laser lighting. Opt. Mater. *121*, 111507.
49. Li, Y.B., Ma, C.Y., Zuo, C.D., Ye, W.G., Shen, X.F., Wang, Y.Z., Li, Y.K., Zhao, C., Wen, Z.C., Yuan, X.Y., and Cao, Y.G. (2021) High thermal stability AlN-YAG: Ce composite phosphor ceramics for highpower laser-driven lighting. Appl. Phys. Lett. *119*, 251903.
50. Peng, X.L, Li, S.X, Zhang, B.H., Liu, Z.H., Zhang, H.H., Chen, X., Tian, R.D., Yao, X.M., Huang, Z.R., Xie, R.-J, and Liu, X.J. (2022). Microstructure tailoring of red-emitting AlN-CaAlSiN3:Eu^{2+} composite phosphor ceramics with higher optical properties for laser lighting. J. Eur. Ceram. Soc. *42*, 3339-3344.
51. Liu, Z., Li, S., Huang, Y., Wang, L., Yao, Y., Long, T., Yao, X., Liu, X., and Huang, Z. (2018). Composite ceramic with high saturation input powder in solid-state laser lighting: Microstructure, properties, and luminous emittances. Ceram. Intern. *44*, 20232-20238.
52. Ji, H., Wang, L., Molokeev, M.S., Hirosaki, N., Huang, Z., Xia, Z., Kate, O.M. ten, Liu, L., and Xie, R.-J. (2016). New garnet structure phosphors, $Lu_{3-x}Y_xMgAl_3SiO_{12}$:$Ce^{3+}$ (x = 0–3), developed by solid solution design. J. Mater. Chem. C *4*, 2359-2366.
53. Zhou, Y., Zhuang, W., Hu, Y., Liu, R., Xu, H., Liu, Y., and Li, Y. (2019). Second-Sphere Polyhedron-Distortion-Induced Broadened and Red-Shifted Emission in $Lu_3(Mg_xAl_{2-x})(Al_{3-x}Si_x)O_{12}$:$Ce^{3+}$ for Warm WLED. Inorganic Chemistry *58*, 9108-9117.
54. Alahraché, S., Deschamps, M., Lambert, J., Suchomel, M.R., De Sousa Meneses, D., Matzen, G., Massiot, D., Véron, E., and Allix, M. (2011). Crystallization of Y_2O_3–Al_2O_3 Rich Glasses: Synthesis of YAG Glass-Ceramics. J. Phys. Chem. C *115*, 20499-20506.
55. Ji, H., Wang, L., Molokeev, M.S., Hirosaki, N., Xie, R.-J., Huang, Z., Xia, Z.,

Kate, O.M.t., Liu, L., and Atuchin, V.V. (2016). Structure evolution and photoluminescence of $Lu_3(Al,Mg)_2(Al,Si)_3O_{12}:Ce^{3+}$ phosphors: new yellow-color converters for blue LED-driven solid state lighting. J. Mater. Chem. C *4*, 6855.

56. Qiao, J., Shen, L., Xiao, W., Qiao, X., Wang, Z., Gao, L., Li, B., Zhou, Y., Zhang, X., and Zhang, X. (2017). Photoluminescence and charge compensation effects in $Lu_3Mg_yAl_{5-x-y}Si_xO_{12}:Ce^{3+}$ phosphors for white LEDs. J. Alloys and Comp. *695*, 567-573.
57. Du, Q., Feng, S., Qin, H., Hua, H., Ding, H., Jia, L., Zhang, Z., Jiang, J., and Jiang, H. (2018). Massive red-shifting of Ce^{3+} emission by Mg^{2+} and Si^{4+} doping of YAG:Ce transparent ceramic phosphors. J. Mater. Chem. C *6*, 12200.
58. Zheng, P., Li, S., Takeda, T., Xu, J., Takahashi, K., Tian, R., Wei, R., Wang, L., Zhou, T.-L., Hirosaki, N., and Xie, R.-J. (2021). Unraveling the Luminescence Quenching of Phosphors under High-Power-Density Excitation. Acta Mater. *209*, 116813.
59. Fujita, S., Umayahara, Y., and Tanabe, S. (2010). Influence of light scattering on luminous efficacy in Ce YAG glass-ceramic phosphor. J. Ceram. Soc. Jpn. *118*, 128-131.
60. Meretska, M.L., Uppu, R., Vissenberg, G., Lagendijk, A., Ijzerman, W.L., and Vos, W.L. (2017). Analytical modeling of light transport in scattering materials with strong absorption. Opt. Express *25*, A906-A921.
61. Zhang, Q., Zheng, R., Ding, J., Cui, P., Wang, Z., Lv, P., and Wei, W. (2021). High lumen density of Al_2O_3-LuAG:Ce composite ceramic for high-brightness display. J. Am. Ceram. Soc. *104*, 3260-3268.
62. Hříbalová, S., and Pabst, W. (2021). Modeling light scattering by spherical pores for calculating the transmittance of transparent ceramics – All you need to know. J. Eur. Ceram. Soc. *41*, 2169-2192.
63. Song, Y. H., Ji, E. K., Jeong, B. W., Jung, M. K., Kim, E. Y., Lee, C. W., and Yoon, D. H. (2017). Design of laser-driven high-efficiency Al_2O_3/YAG:Ce^{3+} ceramic converter for automotive lighting: Fabrication, luminous emittance, and tunable color space. Dyes Pigments *139*, 688-692.
64. Song, Y. H., Kwon, S. B., Jung, M. K., Park, W. K., Yoo, J. H., Lee, C. W., Kang, B. K., Yang, W. S., and Yoon, D. H. (2018). Fabrication design for a high-quality laser diode-based ceramic converter for a laser headlamp application. Ceram. Int. *44*, 1182-1186.

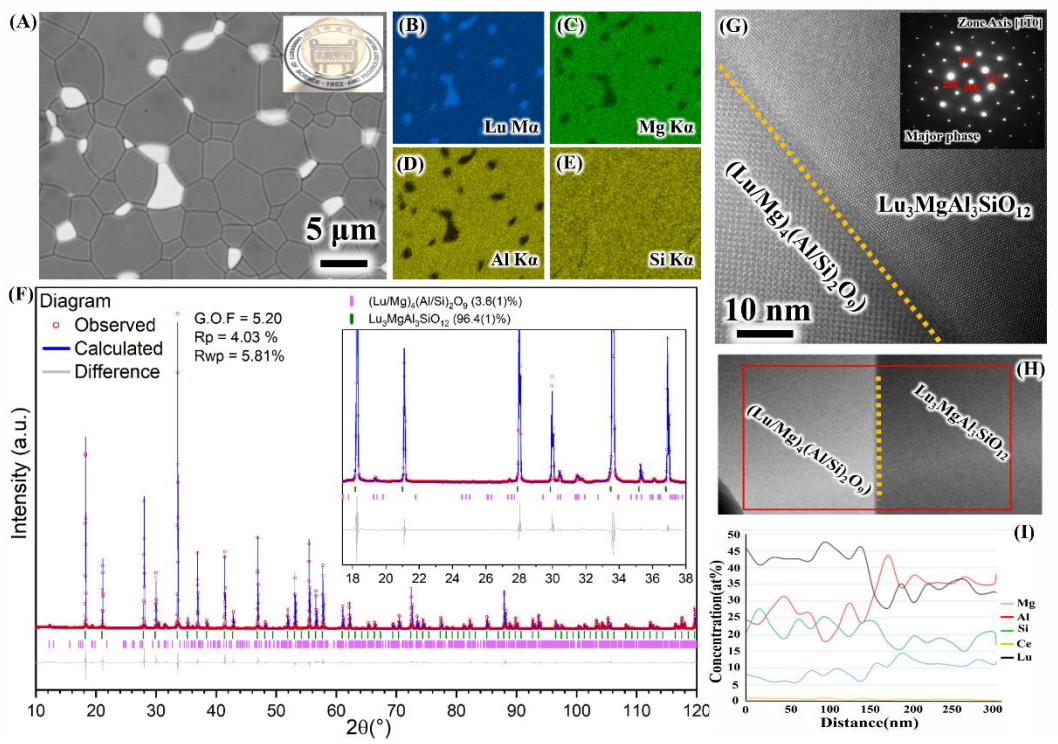

Figure 1. Structure characterizations of BP-LMAS transparent ceramics.

(A) SEM image of the BP-LMAS transparent ceramic with a photograph in the inset.

(B-E) EDS mapping images for the selected region.

(F) Experimental, calculated, and difference XRPD refinement of the BP-LMAS transparent ceramic considering the presence of $Lu_3MgAl_3SiO_{12}$ (96.4(1) wt.%) and $(Lu/Mg)_4(Al/Si)_2O_9$ (3.6(1) wt.%) (Reliability factors for the refinement are GOF = 5.2, Rp = 4.03%, Rwp = 5.81%).

(G) HRTEM image of an interface between the major phase $Lu_3MgAl_3SiO_{12}$ and the secondary phase ($(Lu/Mg)_4(Al/Si)_2O_9$) (scale bar, 10 nm). The related FFT pattern of the major phase is embedded.

(H and I) STEM-EDS cationic composition profile across the corresponding interface (Lu is black, Ce orange, Si green Al red and Mg blue).

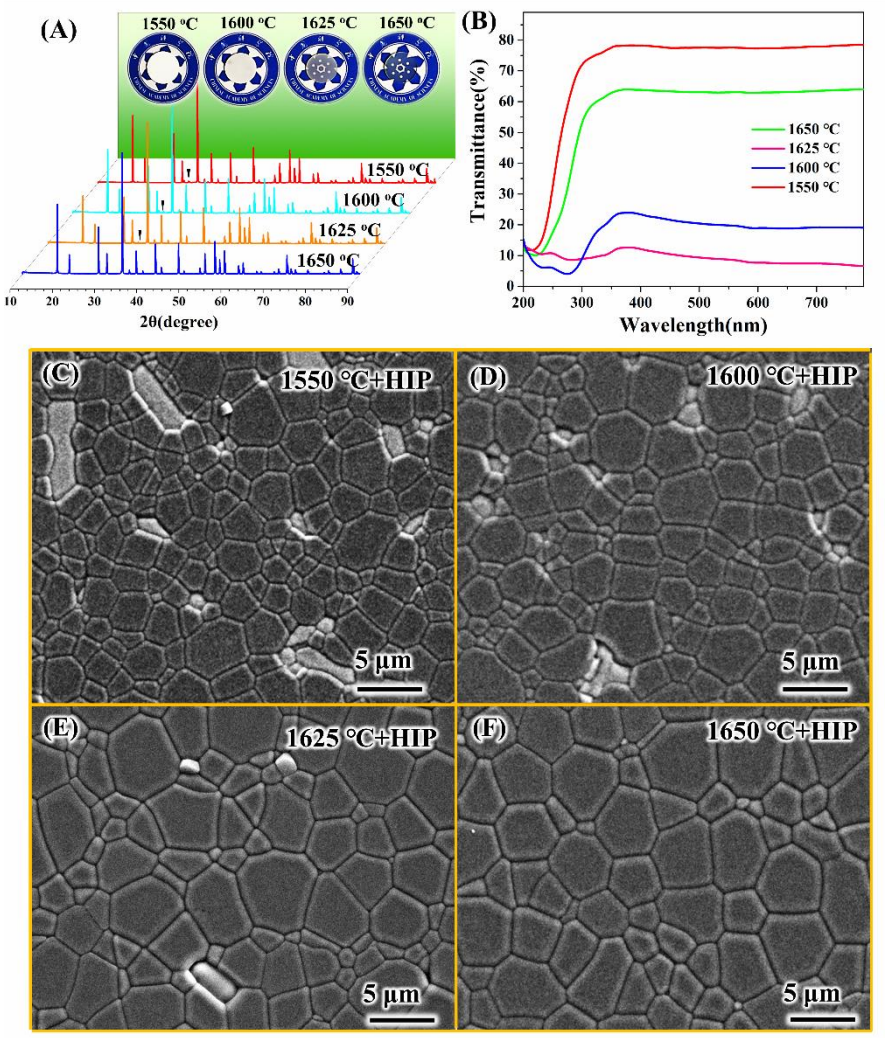

Figure 2. Evolution of BP-LMAS ceramics with sintering temperature increasing.
(A) XRPD patterns of LMAS transparent ceramics pre-sintered at varying temperatures and corresponding photographs in inset.
(B) Transmittance spectra of LMAS transparent ceramics pre-sintered at 1550 °C –1650 °C.
(C-F) SEM images of the LMAS transparent ceramics after 1600 °C/2h and HIP treatment.

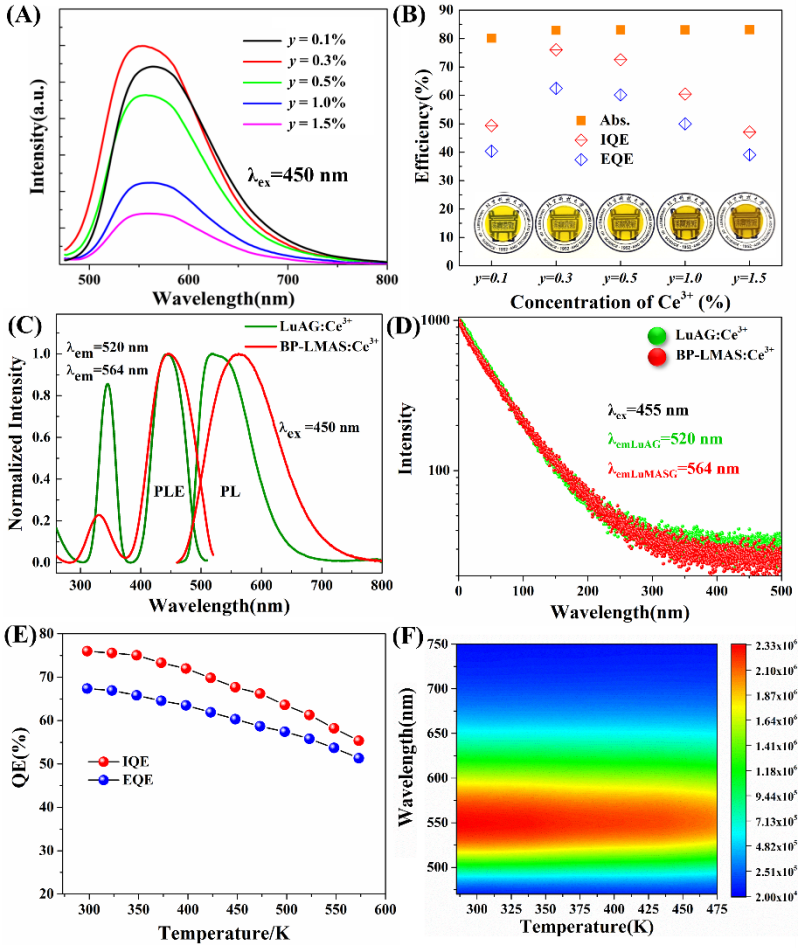

Figure 3. Luminescence properties of BP-LMAS:Ce^{3+}.

(A) PL spectra of BP-LMAS:yCe^{3+} as a function of y = 0.1−1.5%.

(B) Absorption (Abs.) and internal/external quantum efficiency (IQE/EQE).

(C) Normalized photoluminescence excitation (PL) and PL spectra of the BP-LMAS:yCe^{3+} (y = 0.1% to 1.5%) samples. Photographs of all BP-LMAS:yCe^{3+} samples as shown in the inset of b).

(D) Fluorescent decay curves for LuAG:0.3%Ce^{3+} and BP-LMAS:0.3%Ce^{3+} transparent ceramics.

(E) Internal/external quantum efficiency curves with the temperature arising.

(F) Contour plot of thermal quenching behaviors of BP-LMAS:0.3%Ce^{3+} (Above excited by λ_{ex} = 450 nm).

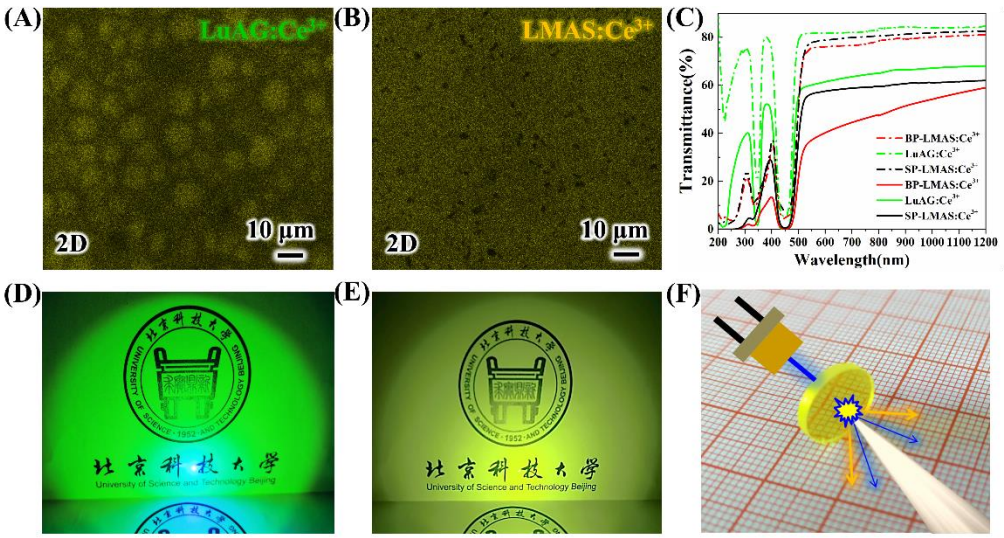

Figure 4. Effect of the secondary phase as light scattering centers.

(A and B) Laser scanning confocal images of LuAG:0.3%Ce^{3+} and BP-LMAS:0.3%Ce^{3+} transparent ceramics.

(C) Transmittance spectra of LuAG:0.3%Ce^{3+} (green), BP-LMAS:0.3%Ce^{3+} (red) and SP- LMAS:0.3%Ce^{3+} (black) transparent ceramics (thickness of 1.0 mm) measured under in-line detector setup (dashed curves) and integrating sphere detector setup (solid line curves). The photograph of samples is shown under 365 nm excitation (inset).

(D and E) Light beam photos of LuAG:0.3%Ce^{3+} and BP-LMAS:0.3%Ce^{3+} transparent ceramics in LDs-driven lighting devices with a transmission mode.

(F) Schematic diagram of LDs-driven lighting devices in a transmission mode.

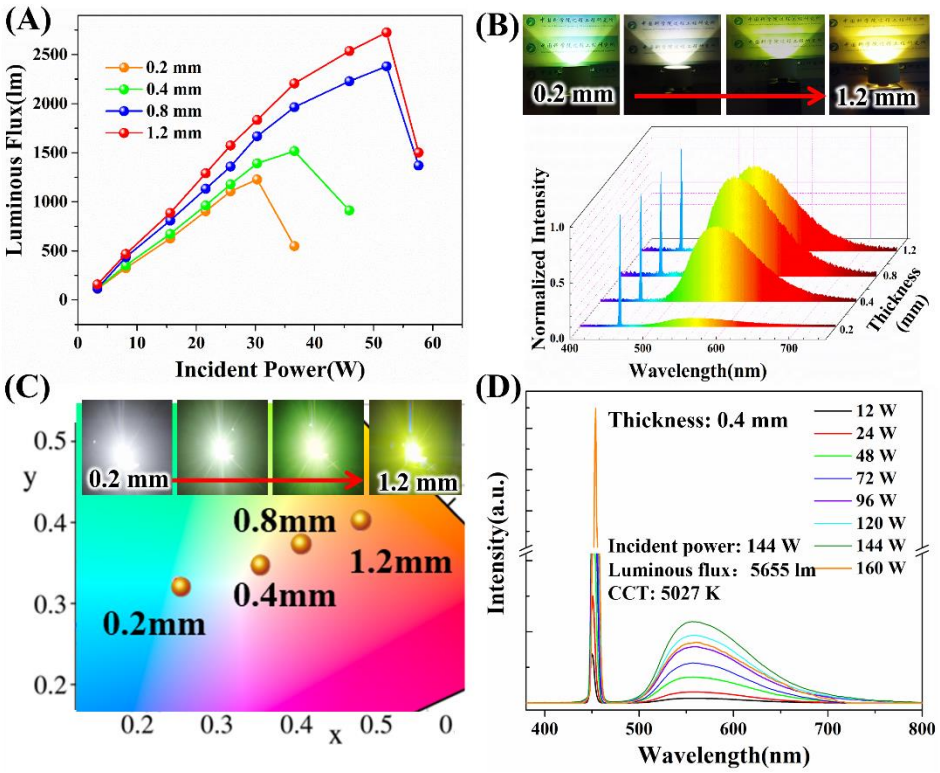

Figure 5. Optical performances of BP-LMAS:0.3% Ce^{3+} transparent ceramics for LDs-driven lighting.

(A and B) Luminous flux as a function of incident power and EL spectra of samples with different thicknesses in a transmission mode under an excitation power of 36.6 W. The top images of (B) revealing photographs of the LDs-driven lighting devices.

(C) Color coordinates of reflective LDs-driven lighting by using ceramics with different thicknesses. Lighting photos are indicated in the top inset.

(D) EL spectra of a reflective mode with a 0.4 mm thick ceramic under different incident powers.